ACS APPLIED MATERIALS & INTERFACES

RESEARCH ARTICLE

www.acsami.org

Micropatterned Arrays of Porous Silicon: Toward Sensory Biointerfaces

Benjamin S. Flavel,* Martin J. Sweetman, Cameron J. Shearer, Joseph G. Shapter, and Nicolas H. Voelcker*

Centre for Nanoscale Science and Technology, School of Chemical and Physical Sciences, Flinders University, Sturt Road, Bedford Park, Adelaide, South Australia, 5001

ABSTRACT:

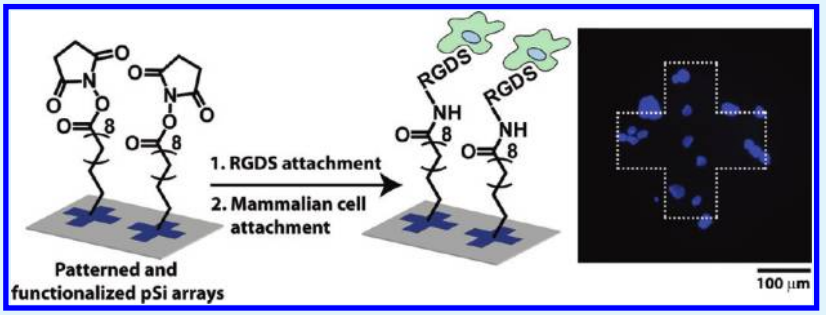

We describe the fabrication of arrays of porous silicon spots by means of photolithography where a positive photoresist serves as a mask during the anodization process. In particular, photoluminescent arrays and porous silicon spots suitable for further chemical modification and the attachment of human cells were created. The produced arrays of porous silicon were chemically modified by means of a thermal hydrosilylation reaction that facilitated immobilization of the fluorescent dye lissamine, and alternatively, the cell adhesion peptide arginine-glycine-aspartic acid-serine. The latter modification enabled the selective attachment of human lens epithelial cells on the peptide functionalized regions of the patterns. This type of surface patterning, using etched porous silicon arrays functionalized with biological recognition elements, presents a new format of interfacing porous silicon with mammalian cells. Porous silicon arrays with photoluminescent properties produced by this patterning strategy also have potential applications as platforms for in situ monitoring of cell behavior.

KEYWORDS: porous silicon, photoluminescence, biointerface, cell adhesion, photolithography

INTRODUCTION

Porous silicon, a material initially reported by Uhlir et al. in 1956[1] as a product of an accidental discovery during silicon wafer machining, and then mostly ignored until a revival of the material by Canham et al. in 1990[2] has since been the subject of a flurry of intense research activity. This is due to potential applications in optoelectronics,[3,4] chemical and biochemical sensing,[5−9] new material supports,[10,11] drug delivery,[12,13] in vivo electronics,[14,15] molecular separation,[16] and surface-enhanced mass spectroscopy.[17−19] Porous silicon is an inorganic material typically produced from crystalline silicon wafers by electrochemical anodization in an electrolyte mixture of hydrofluoric acid (HF), water and ethanol, with (*n*-type) or without (*p*-type) above band gap illumination.[9,20,21] The resulting nanostucture consists of unidirectional aligned pores running perpendicular to the surface.[9] By controlling the current density, crystalline orientation of the wafer, type and concentration of dopant, and electrolyte composition, we can fabricate a variety of different pore morphologies, porosities, and pore sizes.[12,22] The process of pore formation is reproducible, fast, inexpensive, and compatible with standard integrated circuit processes, and leads to a surface with many interesting properties.[22,23] For example, porous silicon exhibits strong Fabry-Pérot fringes[24,25] and has a surface area in the order of 200−500 $m^2\ cm^{-3}$.[23,26] However, two of the most exciting features are its high biocompatibility[9,11−13,25,27−29] and intrinsic photoluminescence.[22,30−33]

A visible red photoluminescence is observed from porous silicon consisting of an ensemble of interconnected nanometre sized silicon crystallites, which have diameters small enough to exhibit quantum confinement.[22] Numerous examples of porous silicon-based optical sensors can be found in the literature utilizing changes in photoluminescence[22,32−34] or reflectivity[7,23,24,35−37] when exposed to target analytes. For example, aromatics such as benzene and anthracene,[38] and nitro-aromatics such as trinitrotoluene and 2,4-dinitrotoluene[39] have been reported to quench the photoluminescence of porous silicon. This principle has been used by Létant et al.[22] who have developed an electronic artificial nose based on porous silicon capable of discriminating between a series of solvent vapors, ethyl esters, and perfumes. In a further example by Létant et al.,[34] the enzyme β-glucuronidase was immobilized to photoluminescent silicon, which demonstrated concentration dependent, reversible

Received: March 21, 2011
Accepted: June 9, 2011
Published: June 09, 2011

quenching of photoluminescence capable of detecting 25 μM p-nitrophenyl-β-D-glucuronide. In contrast, Di Francia et al.[33] have linked single-strand DNA to photoluminescent porous silicon and observed an enhancement in light emission upon complementary strand interaction allowing for detection without labeling steps.

Similarly, porous silicon is finding its niche in cell biology as a biodegradeable support for mammalian cells and tissues.[27,28,40−42] It has long been established that surface topographical cues play an important role in mediating cell orientation and biocompatibility of surfaces[43] with the unique structure of porous silicon proving to be an ideal candidate for the provision of such cues. In fact, Bayliss et al.[40] have shown that porous silicon has a higher viability for various mammalian cell lines compared to glass, polycrystalline silicon or bulk silicon. Furthermore, Low et al.[28] and Khung et al.[44] have demonstrated that surface chemistry and morphological structure of porous silicon play an important role in the adhesion of mammalian cells. Khung et al.[44] have shown that pore size can have a dramatic effect on the ability of cells to adhere to the surface, and that cells prefer large (1−3 μm) to small (100 and 300 nm) pores by comparison. Low et al.[28] showed that for some cell lines amine-functionalization or collagen-coating were required in order to facilitate cell adhesion to porous silicon.

Furthermore it has been shown that porous silicon facilitates close contact with living cells allowing for the direct measurement of cellular signals.[27,45] Predicated on these findings, potential applications such as interfacing of electronics with human neural circuitry, for example enabling reconnection of severed nerve endings[46] are well in sight. At the same time, sensor platforms integrated into cell culture ware will significantly spur discoveries in areas including high-throughput drug testing and stem cell technologies. Schwartz et al.[47] have pioneered the idea of a so-called 'Smart Petridish' where the changes in the optical properties of a porous silicon report on a physiological change occurring in primary rat hepatocytes and *Pseudomonas syringae* bacteria[48] in real time, without interfering with the cells to be studied and with sensitivity exceeding that of traditional cell-based assays.

All of these applications would be considerably enhanced by access to techniques allowing the facile generation of porous silicon patterns.[9] Unfortunately, few examples currently exist in the literature[49−55] of a generic method to reproducibly fabricate porous silicon patterns. Sirbuly et al.[49] have reported a dry removal soft lithography approach where a poly(dimethysiloxane) stamp is adhered to a porous silicon wafer, which upon removal leaves microstructures of porous silicon in the uncontacted regions. In addition, Chattopadhyay et al.[53] and Bao et al.[54] utilized ion beam techniques to create photoluminescent arrays of porous silicon. In turn, Khung et al.[56] used direct ultraviolet laser writing to generate patterned porous silicon. However, the arguably most obvious method to fabricate patterned surfaces is with conventional photolithography. In this area Wang et al.[50] have utilized masks of silicon nitride and silicon carbide. The ceramic coating in these examples was used to ensure substrate pattern retention upon anodization in hydrofluoric acid. More recently, Li et al.[55] have employed a conventional photoresist combined with platinum metal-assisted chemical etching to create a porous silicon based protein microarray. Chen et al.[57] have also used photolithography to create gel pad microarrays templated by patterned porous silicon. Patterned, nanoporous alumina arrays have previously been fabricated through photolithographic techniques and used for mammalian cell culture.[58] The cell adhesion peptide arginine-glycine-aspartic acid (RGD) has been grafted to porous alumina surfaces to enhance cell attachment.[59,60] We perceive two major advantages of using porous silicon over porous alumina in the context of biomaterial and biointerface applications. First, porous silicon is well-known as a biocompatible and biodegradable material and has been investigated as a platform for mammalian cell culture for over a decade.[28,61−65] In contrast to porous alumina, porous silicon completely degrades in aqueous media, with the only product of degradation the nontoxic silicic acid.[66] Second, porous silicon exhibits photoluminescence properties that can be used as a means for noninvasive monitoring of binding events within the pores.[67,68]

In this work, we describe for the first time the use of conventional photolithographic techniques to create arrays of porous silicon by electrochemical anodization without the use of ceramic or metal assistive layers, thereby dramatically reducing the complexity of the fabrication process. The ability to fabricate photoluminescent and nonphotoluminescent porous silicon suitable for further chemical modification by hydrosilylation is demonstrated. Furthermore, immobilization of the dye lissamine, and the cell adhesion peptide arginine-glycine-aspartic acid-serine (RGDS) shows that functionalization of porous silicon arrays with bioactive compounds is feasible. The RGDS-functionalized surface facilitated attachment of human lens epithelial cells. This demonstration of porous silicon patterning and selective cell attachment opens new vistas toward the development of optical sensory components of cell culture systems, which may become viable alternatives to conventional intrusive cell-based assays.

EXPERIMENTAL SECTION

Fabrication of Patterned Porous Silicon Arrays. The procedure for fabrication of patterned porous silicon substrates by the electrochemical etching of silicon in a solution of ethanolic HF is shown schematically in figure 1. First, silicon was cut into 1.5 × 1.5 cm^2 sized wafers and cleaned by ultrasonication (Elmasonic S 30H, Elma Hans Schmidbauer GmbH & Co KG, Germany) in 99.5% acetone (Mallinckrodt Chemicals) for 5 min followed by 5 min in 99.5% isopropyl alcohol (Sigma-Aldrich) with thorough drying with nitrogen gas between each solvent. Immediately after cleaning, positive tone photoresist AZ1518 (Microchemicals, Germany) was spin-coated to a thickness of ∼2 μm at 3000 rpm for 30 s on a WS-400B-6NPP/Lite spinner system (Laurell Technologies Corporation, USA) and soft baked for 60 s at 100 °C on a standard hot plate. An Omnicure S1000 ultraviolet lamp (EXFO Life Sciences and Industrial Division, Canada) was used to pattern the photoresist by a 10 s exposure to 100 W ultraviolet light through a chrome on glass mask (step 1). After exposure, the photoresist was developed by immersion in AZMIF326 developer (Microchemicals, Germany) for 25 s, rinsed with water, dried with dry air (step 2) and immediately transferred to a custom built Teflon etching cell (approximately 1.8 cm^2 working area) and covered with an ethanolic solution of HF. Two etching conditions were followed, one to produce photoluminescent porous silicon and the other for surfaces suitable for dye immobilization or mammalian cell attachment (step 3). Photoluminescent porous silicon surfaces were fabricated from boron doped *p*-type silicon (100) with resistivity 3−6 Ω cm (Silicon Quest International, USA) with an etching solution of 1:4 aqueous HF (48% (w/w), Merck, Germany) to ethanol (100% undenatured, Chem-Supply, Australia). A current of 4 mA was applied for 10 min using a Keithley 2425 source meter (Keithley, USA). Patterned porous silicon for dye immobilization and cell attachment was prepared from boron doped *p*-type silicon (100) with resistivity 0.00055−0.001 Ω cm (Virginia

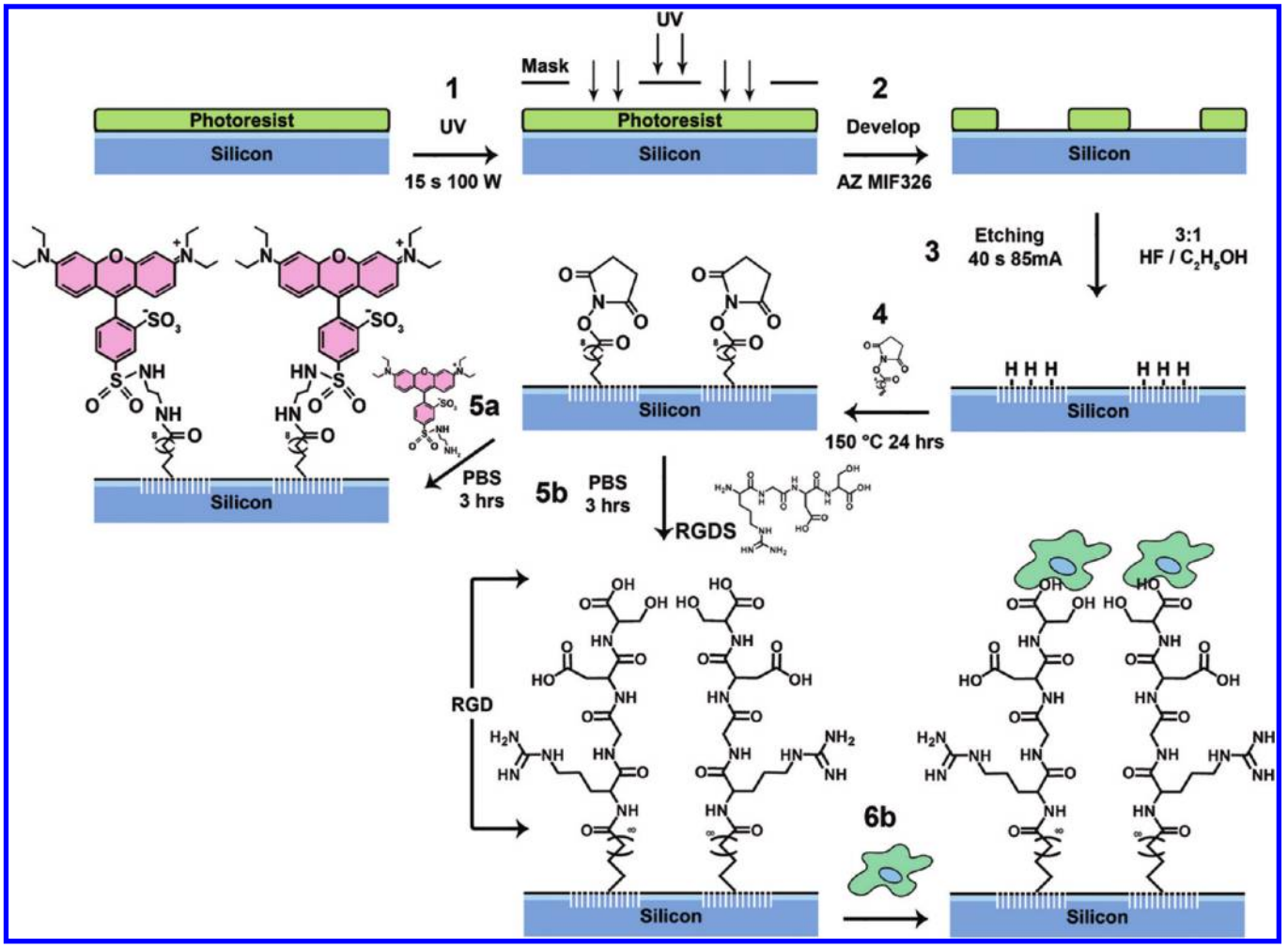

Figure 1. Schematic of porous silicon microarray fabrication and the subsequent immobilization of lissamine dye (5a) and selective attachment of human lens epithelial cells (6b) mediated by an immobilized cell adhesion peptide.

Semiconductor, USA) with an etching solution of 3:1 aqueous HF: ethanol. A current of 85 mA was applied for 40 s. After anodization, the porous silicon was washed sequentially with methanol (Chem-Supply, Australia), acetone and dichloromethane (Chem-Supply, Australia) before being dried under a stream of nitrogen gas.

Surface Modification. For lissamine dye immobilization and cell attachment, patterned porous silicon was further modified by means of thermal hydrosilylation (step 4), where a freshly etched porous silicon surface was immersed in a degassed (three freeze−pump−thaw cycles) 100 mM solution of synthesized N-hydroxysuccinimide alkene (NHS) in mesitylene,[69] under positive argon pressure. The reaction vessel was then sealed, flooded with argon and immersed in an oil bath. The reaction was allowed to proceed at 150 °C for 24 h. After completion of the reaction, the vessel was allowed to cool, before the porous silicon surface was removed and rinsed with copious amounts of dichloromethane and dried under a stream of nitrogen gas. To this surface, either lissamine (step 5a) or arginine-RGDS (step 5b) was covalently attached. The porous silicon surface was allowed to react with either 0.1 mg/mL lissamine (Invitrogen, USA) or 0.1 mg/mL RGDS (Peptides International, USA) in pH 7.4 phosphate buffer saline solution (PBS) for 3 h. After reaction, the surface was washed with PBS solution and Milli-Q water and dried under a stream of nitrogen gas.

Cell Culture. SRA human lens epithelial cells were cultured on the RGDS functionalized surface (step 6b). SRA cells were cultured in Dulbecco's Modified Eagle Medium containing 5 mM L-glutamine, 100 IU/mL penicillin, 100 μg/mL streptomycin sulfate (Invitrogen, USA) and 10% v/v fetal bovine serum (Bovogen Biologicals, Australia) and maintained at 37 °C in 5% CO_2. To investigate cell attachment to the RGDS functionalized surfaces, cells were incubated on the surface at a density of 1×10^5 cells/mL in pH 7.4 PBS solution for 4 h. After this time, the surfaces were rinsed with PBS solution and PBS-Tween (0.05%) to remove any nonspecifically or weakly attached cells. During the final 30 min of incubation, 10 μL of a 200 μg/mL stock solution of Hoechst 33342 (Invitrogen, USA) fluorescent stain was added to the culture medium of each surface.

Microscopy. Scanning electron microscope (SEM) images were obtained using a Helios Nanolab 650 Dual Beam (FEI, USA) with an accelerating voltage of 10 kV. Fluorescence microscopy images were captured with an Eclipse 50*i* microscope equipped with a D-FL universal epi-fluorescence attachment and a 100 W mercury lamp (Nikon Instruments, Japan). Fluorescence images were recorded by a cooled CCD camera (Nikon Instruments, Japan) in darkened conditions with the NIS-elements v3.07 (Nikon Instruments, Japan) software. Patterned arrays of porous silicon and cells were visualized with the use of a 540/25 nm excitation filter and a 605/55 nm emission filter, with patterned cells visualized with a 340−380 nm excitation filter and a 435−485 nm emission filter.

Spectroscopy. Fluorescence spectroscopy measurements were performed with a Cary Eclipse fluorescence spectrometer (Varian Inc., USA). Operating in fluorescence/emission mode with emission and

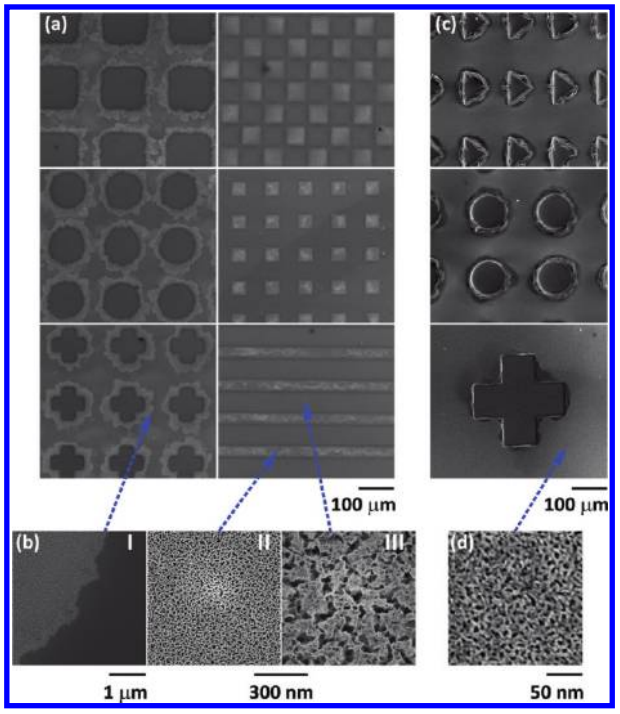

Figure 2. (a, b) Scanning electron microscopy images of patterned nonphotoluminescent porous silicon, and (c, d) photoluminescent porous silicon patterns; b-III corresponds to the patterned porous silicon area.

excitation slit widths of 5 nm, a patterned photoluminescent porous silicon substrate was mounted inside a quartz cuvette and excited with 312 nm light. Infrared spectroscopy measurements were performed on a Nicolet Avatar 370MCT spectrometer (Thermo Electron Corporation, USA). The spectrometer was fitted with a transmission accessory and all spectra were recorded and analyzed using OMNIC version 7 software. Spectra were recorded over a range of 650−4000 cm^{-1}, at a resolution of 2 cm^{-1} and taken as an average of 64 scans. All samples were blanked to a clean unetched and non- functionalized silicon wafer.

RESULTS AND DISCUSSION

The conventional photoresist AZ1518 was spin coated onto *p*-type silicon (100). Patterns with simple geometric shapes (squares, circles, crosses and lines) of dimensions as low as 15 μm were transferred into the resist layer by exposure to ultraviolet light through chrome-on-glass masks. These patterned shapes allowed for selective exposure of the silicon substrate to an ethanolic HF solution during electrochemical etching to afford patterned porous silicon. By changing the resistivity of the silicon substrate, HF concentration, etching time and current density it was possible to fabricate not only patterned arrays of nonphotoluminescent, but also photoluminescent porous silicon. By etching 0.00055−0.001 Ω cm silicon for 45 s with a current of 85 mA in a 3:1 aqueous HF/ethanol solution, patterns of nonphotoluminescent porous silicon were formed. Figure 2a shows scanning electron microscopy images of the resulting structures where a silicon surface consisting of three distinctly different morphologies can be seen. These different morphologies are enlarged in Figure 2b. Surrounding each patterned porous silicon shape is flat crystalline silicon, and the interface between these two regions can clearly be seen, Figure 2b-I. However each shape consisted of two different types of porous silicon, a central region with pores of approximately 35 − 105 nm in diameter, Figure 2b-III, surrounded by an area consisting of smaller pores of approximately 12 − 38 nm in diameter, Figure 2b-II. The region of smaller pores is attributed to dissolution of the photoresist around the edges of the patterns by the ethanolic HF solution during anodization. This diffuse region typically extends 20−40 μm outside the central porous silicon area. For photoresist patterns below this length scale such as the 15 μm "checker board" and line pattern, Figure 2a, this resulted in a surface of alternating large and small pore size porous silicon.

To gain a more complete understanding of the surface structure, we fractured the silicon substrate along the edge of a porous silicon feature allowing for cross-sectional images to be obtained. Figure 3a shows a scanning electron microscope image of a nonphotoluminescent cross-shaped porous silicon feature where the central porous area was 2.74 μm thick and tapered out over 16.6 μm toward the edge of the pattern. Within this tapered region, the porous silicon retained the structure and pore size of the central area. Surrounding the tapered region, porous silicon with pore size as shown in Figure 2b-II was formed with a depth of approximately 14 nm before terminating in flat silicon. This tapering effect can be attributed to the combined effect of undercut etching, experienced when performing masked etching on semiconductor silicon surfaces[70] and the photoresist dissolution. In the case of insulating etching masks (such as the photoresist mask used here), undercut etching occurs as the electric field is forced to pass through the patterned gaps in the mask.[71] This leads to the etching of the silicon in the areas underneath the mask at the edges of the patterned areas.[72] This undercut etching can be clearly seen in Figure 3a, where the undercut etching extends out 16.6 μm from the patterned feature. The thin, small pore region Figure 2b-II and Figure 3a is attributed to the photoresist dissolution around the edges of the patterned features.

Upon etching 3−6 Ω cm silicon for 10 min with a current of 4 mA in a 1:4 aqueous HF/ethanol solution patterns of photoluminescent silicon were produced as shown in Figure 2c and Figure 3b. In this instance, because of the small pore size of the central photoluminescent region, it was not possible to measure pore diameter accurately with the scanning electron microscope. Such small pore sizes are to be expected due to the very low etching current, with these pores exhibiting quantum confinement effects necessary for the porous silicon to be photoluminescent.[2] Because of etching time required to fabricate photoluminescent porous silicon, complete dissolution of the photoresist was observed, and the underlying surface was therefore also etched and showed pores with a diameter of approximately 4 nm, as shown in Figure 2d. These areas did not photoluminesce. Although this pore size here was small compared to the nonphotoluminescent porous silicon described earlier, it was still too large to exhibit quantum confinement.

Upon examination of cross sections of the photoluminescent porous silicon, tapering effects were also observed (Figure 3b). As previously shown in images c and d in Figure 2, nonphotoluminescent porous silicon surrounded the patterned photoluminescent region and was found to exist with a depth of 1.2 μm. However, in this instance, the patterned photoluminescent region was found to be recessed 4.45 μm below the initial height of the silicon substrate. Figure 3b reveals that the patterned porous silicon region is 440 nm thick. Our explanation for the recessed porous silicon regions is as follows: during the initial stages of anodization, a layer of photoluminescent porous silicon is fabricated within the regions not covered by photoresist,

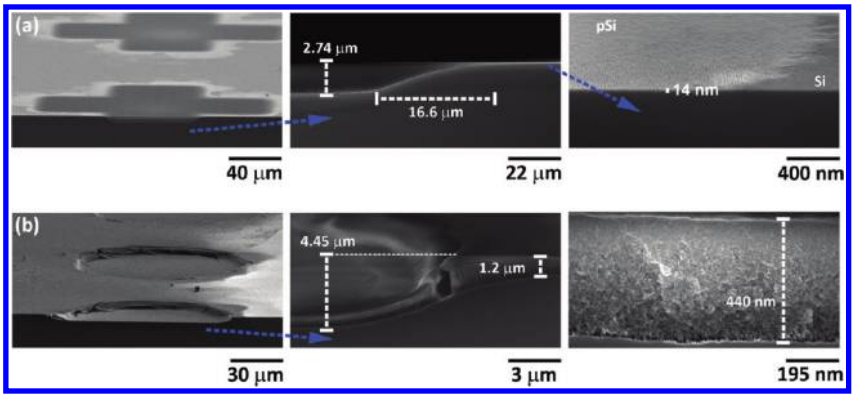

Figure 3. Cross-sectional scanning electron microscopy images of patterned (a) nonphotoluminescent and (b) photoluminescent porous silicon.

whereas the resist-covered silicon is protected. However, over time, the photoresist dissolves and the etching conditions change. First, the total surface area of exposed silicon increases upon photoresist dissolution, which causes a drop in the overall current density at the silicon surface due to the use of a constant current power supply. Second, the already low HF concentration at the pore etching front decreases further as it is consumed in the formation of new pores. Both of these changed parameters result in the dissolution (electropolishing) of the patterned photoluminescent silicon. Furthermore, the changed parameters result in a shift to a new etching regime causing larger pores to be formed around the photoluminescent patterns. Upon comparison of photoluminescent patterns etched for different times it was observed that increasing the etching time resulted in patterns recessed deeper into the silicon substrate. For photoluminescent patterns etched at similar times to nonphotoluminescent patterns it was possible to avoid any recession. However, the photoluminescent intensity was very low. Solid state fluorescence spectroscopy was performed on the photoluminescent patterns and showed an emission peak of 625 nm upon irradiation with 312 nm light as shown in Figure 4a. This peak is in agreement with literature values for photoluminescent porous silicon.[73] Fluorescence microscopy images of the photoluminescent patterns were also found to be well-defined as shown in Figure 5a. As previously discussed, the porous regions surrounding the patterned shapes did not luminesce. We believe that these photoluminescent arrays of porous silicon spots may find applications as biocompatible optical sensor arrays.[74,75]

To demonstrate the feasibility of functionalizing patterned porous silicon regions, the fluorescent dye lissamine and the cell adhesion peptide RGDS were immobilized in separate experiments by means of hydrosilylation chemistry. By performing a hydrosilylation reaction on the freshly etched porous silicon patterns, a functionalized alkene compound only conjugates to the porous surface of the etched areas that have Si−H functionality. This means that the porous silicon surface is selectively functionalized over the surrounding flat silicon surface that has not come into contact with HF and retains its native silicon oxide functionality. Hydrosilylation reactions and further functionalizations were only carried out on the nonphotoluminescent porous silicon surfaces. This type of surface functionalization reaction has been demonstrated to produce stable porous silicon surfaces, able to last for extended time in aqueous media.[61,76] The surface modifications were followed by transmission infrared spectroscopy as shown in Figure 4. Figure 4b shows a series of infrared spectra corresponding to each step in the surface modification for producing the RGDS functionalized surfaces. The spectra correspond to freshly etched porous silicon, N-hydroxysuccinimide (NHS) ester functionalized porous silicon, and RGDS-functionalized porous silicon before and after quenching of the NHS residues that had not reacted with the peptide using ethanolamine. Methylene stretching vibrations around 2900 cm^{-1} confirm the successful attachment of the alkene species to the porous silicon surface using thermal hydrosilylation.[77] A large reduction in the intensity of Si−H stretching vibrations at 2100 cm^{-1} also confirms successful reaction of the initial hydride terminated porous silicon surface.[78] The peaks at 2230 and 1100 cm^{-1} correspond to oxygen backbonded Si−H and Si−O, respectively.[79] These peaks are representative of surface oxidation, which commonly occurs as a side reaction during thermal hydrosilylation.[80] Figure 4c displays an enlarged section of the infrared spectra that allows for changes in the carbonyl stretching vibrations to be easily visualized. The spectra corresponding to the NHS ester functionalized porous silicon surface shows a set of three peaks between 1850 and 1700 cm^{-1} that correspond to the carbonyl stretching vibration of the ester (1810 cm^{-1}) and the symmetric and asymmetric stretching of the NHS ester carbonyls (1780 and 1730 cm^{-1}, respectively).[79,81] We observed that after the RGDS is immobilized on the surface the intensity of these carbonyl peaks (especially the peaks at 1780 and 1810 cm^{-1} associated with the symmetric and ester carbonyl stretching of the NHS) is reduced. Following RGDS immobilization, the peak around 1730 cm^{-1} has broadened, consistent with the presence of carbonyl stretching bands of the peptide, and there is a small peak present at 1530 cm^{-1} which corresponds to N−H bending modes of amide II vibrations.[82] The reduction of the NHS carbonyl peak intensity and the presence of the amide bond indicate the successful attachment of the RGDS to the NHS ester. After the surface was reacted with ethanolamine, it was observed that the NHS ester carbonyl peak had almost disappeared, indicating successful quenching of the remaining NHS ester functionalities on the functionalized porous silicon surface. Figure 4d,e show the infrared spectra series for lissamine dye immobilization on the porous silicon surface. The spectra in panels d and e in Figure 4 are almost identical to those in b and c in Figure 4. After reaction with lissamine, a conspicuous amide I peak at 1650 cm^{-1} appeared, indicating the successful attachment of the amino functional dye to the surface. The expanded spectral window in Figure 4e shows further vibrational peaks, which we attributed to other functional groups of the lissamine dye (such as sulphones and sulphonamides).[83]

Fluorescence microscopy was used to visualize the porous silicon patterns after lissamine functionalization. In Figure 5b,

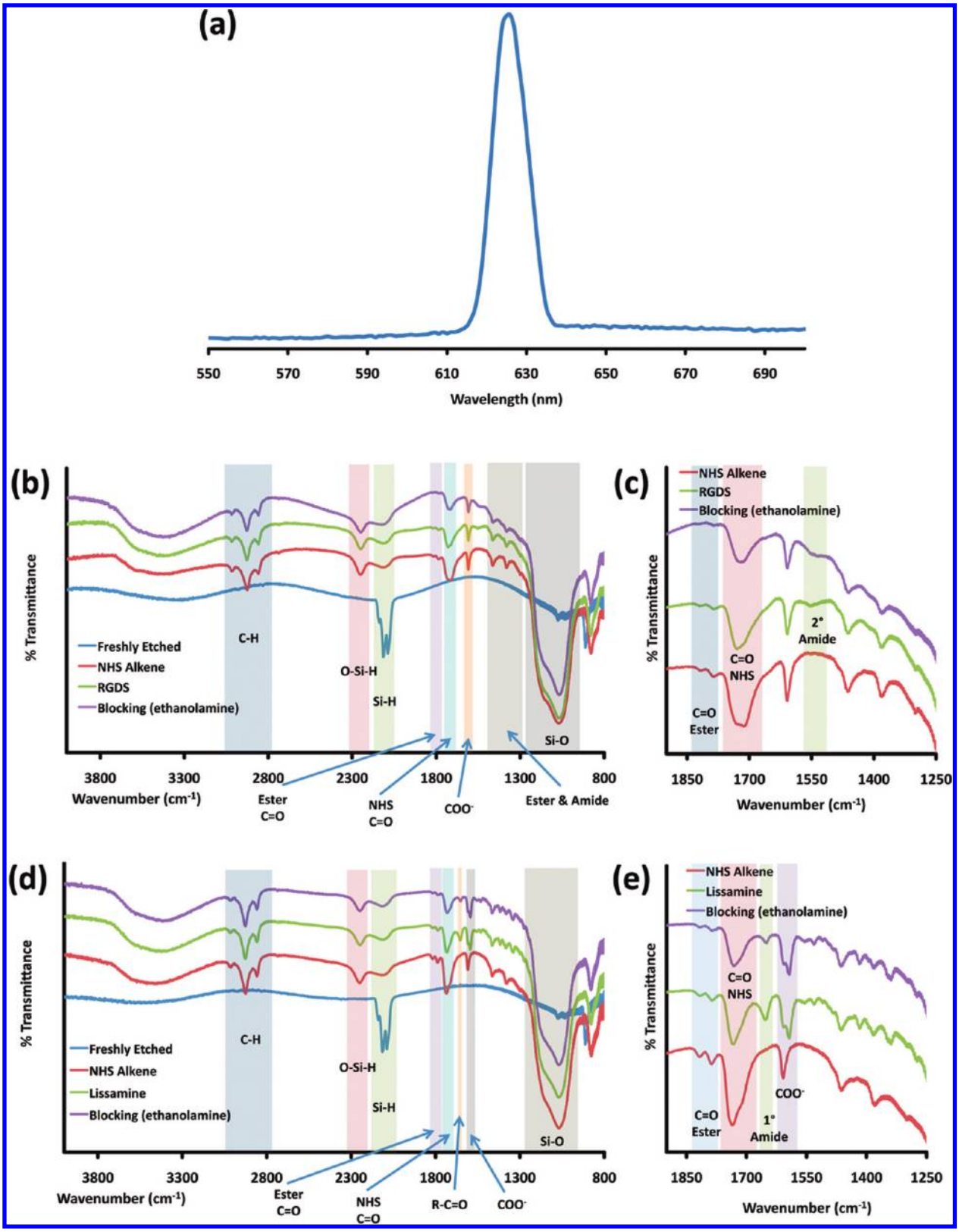

Figure 4. (a) Fluorescence spectrum of photoluminescent porous silicon. Transmission infrared spectra of various porous silicon surface modifications resulting in the immobilization of (b, c) RGDS and (d, e) lissamine.

highly defined arrays of lissamine functionalized porous silicon were observed. This is in contrast to the poorly defined patterns due to electric field decay and photoresist removal seen by scanning electron microscope in images a and b in Figure 2. The observed difference can be simply explained by considering the available surface area for lissamine modification. The high

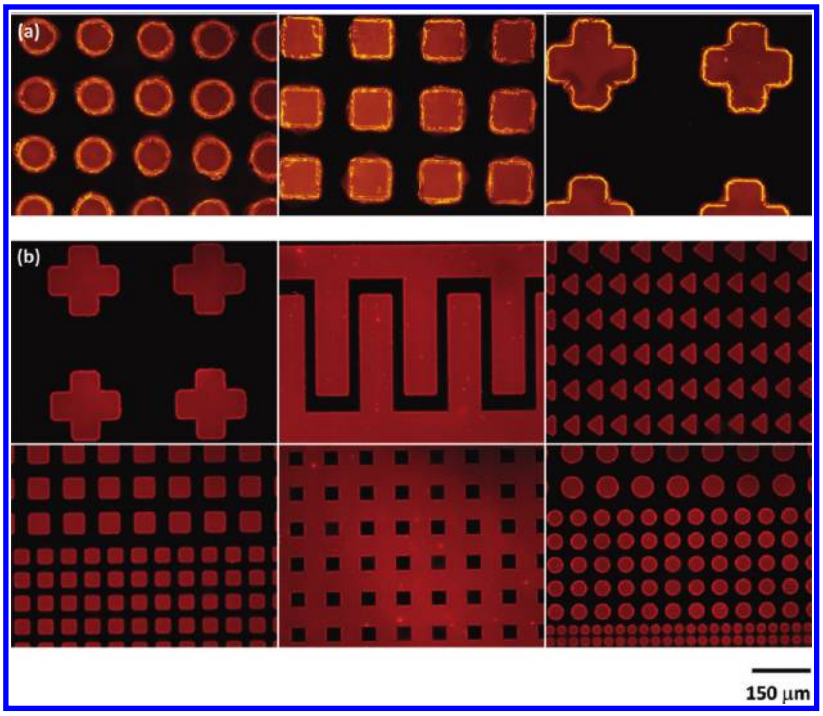

Figure 5. (a) Fluorescence microscopy images of patterned photoluminescent porous silicon and (b) nonphotoluminescent patterned porous silicon after lissamine immobilization.

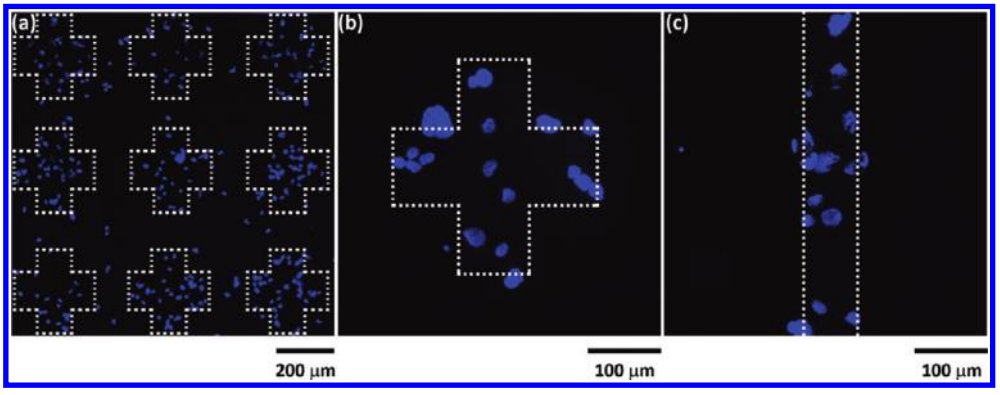

Figure 6. Fluorescence microscopy images of Hoechst 33342 stained human lens epithelial cells on patterned porous silicon arrays (patterns are highlighted by dotted lines, which serve as a guide to the eye).

etch depth of the central region (2.74 μm) as compared to the thin surrounding areas (14 nm) allow for significantly more lissamine loading in the central regions as opposed to the periphery. This results in a strong fluorescence contrast between the central and the surrounding regions.

To demonstrate the response of mammalian cells to the generated RGDS functionalized porous silicon, we incubated surfaces with human lens epithelial cells at a cell seeding density of 1×10^5 cells/mL. This particular cell line was chosen because of our interest in developing cell-based assays on primary ocular cells in culture.[42] To visualize cell attachment to the patterned porous silicon arrays, the cell nuclei were stained with Hoechst 33342. Cell attachment was visualized using fluorescence microscopy as shown in Figure 6. The characteristic blue fluorescence of the Hoechst 33342 stained cell nucleus can clearly be seen. To aid the eye, patterned porous silicon regions are highlighted in the figure with a dotted line. By counting the number of cells immobilized within a patterned region and comparing it to the number of cells nonspecifically bound to the flat silicon it was found that 90% of all cells were bound within the porous silicon regions. A higher density of cells within the patterned region is expected, since the RGDS sequence is known to interact with the extracellular regions of integrins in the cell membrane and helps to anchor the cells to the surface.[84] Washing of the incubated surface with PBS and PBS-Tween (0.05%) removed most of the nonspecifically or weakly bound cells, leaving behind only cells that were strongly attached to the surfaces. It should be noted that no attempt had been made to incorporate low-fouling coatings on the flat silicon surface, for example using silanization with polyethylene glycol silanes.[85] For this reason, cell adhesion to the functionalized surfaces was carried out in PBS in the absence of serum proteins, to negate the effects of proteins nonspecifically adsorbing to the silicon surface and influencing cell attachment. Only a short (4 h) incubation time was used to

investigate cell attachment to the functionalized porous silicon arrays. Cell morphology and proliferation on these arrays were not investigated as part of this study.

CONCLUSION

This work has demonstrated a simple, photolithographic method for the fabrication of patterns of porous silicon. Attractive features of this method include that the use of ceramic coatings such as silicon carbide or the use of additional metal layers for metal-assisted etching are not necessary. Furthermore, the method is suitable for rapid patterning of large surface areas. Arrays of photoluminescent and nonphotoluminescent porous silicon have been demonstrated. Photoluminescent arrays of porous silicon are expected to have applications in the fabrication of optical sensing systems where changes in photoluminescence will be used to detect target analyte molecules. On nonphotoluminescent porous silicon, selective chemical functionalization was demonstrated by the immobilization of lissamine and RGDS after thermal hydrosilylation with an NHS ester-terminal alkene on the porous regions. We demonstrate that human lens epithelial cells selectively attach to the RGDS functionalized patterned porous silicon. Taken together, our results constitute a significant advance in our efforts of developing optical sensor arrays interfaced with mammalian cells in culture for nonintrusive detection of cellular processes.

AUTHOR INFORMATION

Corresponding Author

*E-mail: ben.flavel@flinders.edu.au (B.S.F.); nico.voelcker@flinders.edu.au (N.H.V.).

ACKNOWLEDGMENT

Authors gratefully acknowledge the support of the South Australian node of the Australian Microscopy & Microanalysis Research Facility (AMMRF) for access to the Helios Nanolab scanning electron microscope. Authors thank Mr. Yazad Irani for preparation of the epithelial cell line, supplied by and used with permission from Professor Venkat Reddy from the Kellogg Eye Centre, University of Michigan, Ann Arbor, MI, USA. This work was supported by the Australian Research Council.

REFERENCES

(1) Uhlir, A. *Bell Syst. Technol. J.* **1956**, *35*, 333.
(2) Canham, L. T. *Appl. Phys. Lett.* **1990**, *57*, 1046–1048.
(3) Cullis, A. G.; Canham, L. T.; Calcott, P. D. J. *J. Appl. Phys.* **1997**, *82*, 909–965.
(4) Brus, L. *J. Phys. Chem.* **1994**, *98*, 3575–3581.
(5) Létant, S. E.; Sailor, M. J. *Adv. Mater.* **2000**, *12*, 355.
(6) Zangooie, S.; Bjorklund, R.; Arwin, H. *Sens. Actuators, B* **1997**, *43*, 168.
(7) Dancil, K. P. S.; Greiner, D. P.; Sailor, M. J. *J. Am. Chem. Soc.* **1999**, *121*, 7925–7930.
(8) Starodub, V. M.; Fedorenko, L. L.; Sisetskiy, A. P.; Starodub, N. F. *Sens. Actuators B* **1999**, *58*, 409.
(9) Jane, A.; Dronov, R.; Hodges, A.; Voelcker, N. H. *Trends Biotechnol.* **2009**, *27*, 230–238.
(10) Fan, S.; Chapline, M. G.; Franklin, N. R.; Tombler, T. W.; Cassell, A. M.; Dai, H. *Science* **1999**, *283*, 512.
(11) Nussio, M.; Oncins, G.; Ridelis, I.; Szili, E.; Shapter, J.; Sanz, F.; Voelcker, N. H. *J. Phys. Chem.* **2009**, *113*, 10339–10347.
(12) Anglin, E. J.; Cheng, L.; Freeman, W. R.; Sailor, M. J. *Adv. Drug Delivery Rev.* **2008**, *60*, 1266–1277.
(13) McInnes, S.; Voelcker, N. H. *Future Med. Chem.* **2009**, *1*, 1051–1074.
(14) Canham, L. T. *Adv. Mater.* **1995**, *7*, 1033.
(15) Li, X.; Coffer, J. L.; Chen, Y. D.; Pinizzotto, R. F.; Newey, J.; Canham, L. T. *J. Am. Chem. Soc.* **1998**, *120*, 11706.
(16) Velleman, L.; Shearer, C.; Voelcker, N. H.; Shapter, J. G. *Nanoscale* **2010**, *2*, 1756–1761.
(17) Wei, J.; Buriak, J. M.; Siuzdak, G. *Nature* **1999**, *399*, 243.
(18) Lowe, R. D.; Guild, G.; Harpas, P.; Kirkbride, P.; Hoffmann, P.; Voelcker, N. H.; Kobus, H. *Rapid Commun. Mass Spectrom.* **2009**, *23*, 3543–3548.
(19) Lowe, R. D.; Szili, E. J.; Kirkbride, P.; Thissen, H.; Siuzdak, G.; Voelcker, N. H. *Anal. Chem.* **2010**, *82*, 4201–4208.
(20) Lau, H. W.; Parker, G. J.; Greef, R.; Hölling, M. *Appl. Phys. Lett.* **1995**, *67*, 1877–1879.
(21) Li, X.; Bohn, P. W. *Appl. Phys. Lett.* **2000**, *77*, 2572–2574.
(22) Létant, S. E.; Content, S.; Tan, T. T.; Zenhausern, F.; Sailor, M. J. *Sens. Actuators B* **2000**, *69*, 193–198.
(23) Stefano, L. D.; Rotiroti, L.; Rendina, I.; Moretti, L.; Scognamiglio, V.; Rossi, M.; Auria, S. D. *Biosens. Bioelectron.* **2006**, *21*, 1664–1667.
(24) Lin, V. S.-Y.; Motesharei, K.; Dancil, K.-P. S.; Sailor, M. J.; Ghadiri, M. *Science* **1997**, *278*, 840–843.
(25) Stewart, M. P.; Buriak, J. M. *Adv. Mater.* **2000**, *12*, 859–869.
(26) Singh, S.; Sharma, S. N.; Govind; Shivaprasad, S. M.; Lal, M.; Khan, M. A. *J. Mater. Sci. Mater. Med.* **2009**, *20*, S181–S187.
(27) Sapelkin, A. V.; Bayliss, S. C.; Unal, B.; Charalambou, A. *Biomaterials* **2006**, *27*, 842–846.
(28) Low, S. P.; Williams, K. A.; Canham, L. T.; Voelcker, N. H. *Biomaterials* **2006**, *27*, 4538–4546.
(29) Salonen, J.; Lehto, V.-P. *Chem. Eng. J.* **2008**, *137*, 162–172.
(30) Bisi, O.; Ossicini, S.; Pavesi, L. *Surf. Sci. Rep.* **2000**, *38*, 1–126.
(31) Föll, H.; Christophersen, M.; Carstensen, J.; Hasse, G. *Mater. Sci. Eng., R* **2002**, *39*, 93–141.
(32) Seals, L.; Gole, J. L.; Tse, L. A.; Hesketh, P. J. *J. Appl. Phys.* **2002**, *91*, 2519–2523.
(33) Francia, G. D.; Ferrara, V. L.; Manzo, S.; Chiavarini, S. *Biosens. Bioelectron.* **2005**, *21*, 661–665.
(34) Létant, S. E.; Hart, B. R.; Kane, S. R.; Hadi, M. Z.; Sheilds, S. J.; Reynolds, J. G. *Adv. Mater.* **2004**, *16*, 689–693.
(35) Worsfold, O.; Voelcker, N. H.; Nishiya, T. *Langmuir* **2006**, *22*, 7078–7083.
(36) Voelcker, N. H.; Alfonso, I.; Ghadiri, M. R. *ChemBioChem* **2008**, *9*, 1176–1786.
(37) Lin, V. S.-Y.; Janshoff, A.; Steinem, C.; Voelcker, N. H.; Ghadiri, M. R. *Tetrahedron* **2004**, *60*, 11259–11267.
(38) Song, J. H.; Sailor, M. J. *J. Am. Chem. Soc.* **1997**, *119*, 7381.
(39) Content, S.; Trogler, W. C.; Sailor, M. J. *Chem.—Eur. J.* **2000**, *6*, 2205.
(40) Bayliss, S. C.; Heald, R.; Fletcher, I.; Buckberry, L. D. *Adv. Mater.* **1999**, *11*, 318.
(41) Bayliss, S. C.; Buckberry, L. D.; Harris, P. J.; Rousseau, C. *Thin Solid Films* **1997**, *297*, 308.
(42) Low, S. P.; Voelcker, N. H.; Canham, L. T.; Williams, K. A. *Biomaterials* **2009**, *30*, 2873–2880.
(43) Craighead, H. G.; James, C. D.; Turner, A. M. P. *Curr. Opin. Solid State Mater. Sci.* **2001**, *5*, 117–184.
(44) Khung, Y. L.; Barritt, G.; Voelcker, N. H. *Exp. Cell Res.* **2008**, *314*, 789–800.
(45) Mayne, A. H.; Bayliss, S. C.; Barr, P.; Tobin, M.; Buckberry, L. D. *Phys. Status Solidi A* **2000**, *182*, 505–513.
(46) Heiduschka, P.; Thanos, S. *Prog. Neurobiol.* **1998**, *55*, 433.
(47) Schwartz, M. P.; Derfus, A. M.; Alvarez, S. D.; Bhatia, S. N.; Sailor, M. J. *Langmuir* **2006**, *22*, 7084–7090.
(48) Alvarez, S. D.; Schwartz, M. P.; Migliori, B.; Rang, C. U.; Chao, L.; Sailor, M. J. *Phys. Status Solidi A* **2007**, *204*, 1439–1443.

(49) Sirbuly, D. J.; Lowman, G. M.; Scott, B.; Stucky, G. D.; Buratto, S. K. *Adv. Mater.* **2003**, *15*, 149–152.
(50) Wang, H.; Welker, B.; Gao, Y.; Federici, J. F.; Levy, R. A. *Mater. Lett.* **1995**, *23*, 209–214.
(51) Ohmukai, M.; Okada, K.; Tstusumi, Y. *J. Mater. Sci.: Mater. Electron.* **2005**, *16*, 119–121.
(52) Nassiopoulos, A. G.; Grigoropoulos, S.; Canham, L.; Halimaoui, A.; Berbezier, I.; Gogolides, E.; Papadimitriou, D. *Thin Solid Films* **1995**, *255*, 329–333.
(53) Chattopadhyay, S.; Bohn, P. W. *J. Appl. Phys.* **2004**, *96*, 6888–6894.
(54) Bao, X.-M.; Yang, H.-Q. *Appl. Phys. Lett.* **1993**, *63*, 2246–2247.
(55) Li, H.-F.; Han, H.-M.; Wu, Y.-G.; Xiao, S.-J. *Appl. Surf. Sci.* **2010**, *256*, 4048–4051.
(56) Khung, Y. L.; Graney, S.; Voelcker, N. H. *Biotechnol. Prog.* **2006**, *22*, 1388–1393.
(57) Chen, L.; Chen, Z.-T.; Wang, J.; Xiao, S.-J.; Lu, Z.-H.; Gu, Z.-Z.; Kang, L.; Chen, J.; Wu, P.-H.; Tang, Y.-C.; Liu, J.-N. *Lab Chip* **2009**, *9*, 756–760.
(58) Swan, E. E. L.; Popat, K. C.; Grimes, C. A.; Desai, T. A. *J. Biomed. Mater. Res. Part A* **2005**, *72A*, 288–295.
(59) Lee, H. J.; Kim, D. N.; Park, S.; Lee, Y.; Koh, W.-G. *Acta Biomater.* **2011**, *7*, 1281–1289.
(60) Leary Swan, E. E.; Popat, K. C.; Desai, T. A. *Biomaterials* **2005**, *26*, 1969–1976.
(61) Sweetman, M. J.; Harding, F. J.; Graney, S. D.; Voelcker, N. H. *Appl. Surf. Sci.* **2011**, *257*, 6768–6774.
(62) Low, S. P.; Voelcker, N. H.; Canham, L. T.; Williams, K. A. *Biomaterials* **2009**, *30*, 2873–2880.
(63) de-Leon, S. B.-T.; Oren, R.; Spira, M. E.; Korbakov, N.; Yitzchaik, S.; Sa'ar, A. *Phys. Status Solidi A* **2005**, *202*, 1456–1461.
(64) Chin, V.; Collins, B. E.; Sailor, M. J.; Bhatia, S. N. *Adv. Mater.* **2001**, *13*, 1877–1880.
(65) Bayliss, S. C.; Heald, R.; Fletcher, D. I.; Buckberry, L. D. *Adv. Mater.* **1999**, *11*, 318–321.
(66) Mayne, A. H.; Bayliss, S. C.; Barr, P.; Tobin, M.; Buckberry, L. D. *Phys. Stat. Sol. A* **2000**, *182*, 505–515.
(67) Rea, I.; Lamberti, A.; Rendina, I.; Coppola, G.; Gioffrè, M.; Iodice, M.; Casalino, M.; De Tommasi, E.; De Stefano, L. *J. Appl. Phys.* **2010**, *107*, 014513–1 - 014513−4.
(68) Kilian, K. A.; Lai, L. M. H.; Magenau, A.; Cartland, S.; Bocking, T.; Di Girolamo, N.; Gal, M.; Gaus, K.; Gooding, J. J. *Nano Lett.* **2009**, *9*, 2021–2025.
(69) Yin, H. B.; Brown, T.; Greef, R.; Wilkinson, J. S.; Melvin, T. *Microelectron. Eng.* **2004**, *73−74*, 830–836.
(70) Kruger, M.; Arens-Fischer, R.; Thonissen, M.; Munder, H.; Berger, M. G.; Luth, H.; Hilbrich, S.; Theiss, W. *Thin Solid Films* **1996**, *276*, 257–260.
(71) Steiner, P.; Lang, W. *Thin Solid Films* **1995**, *255*, 52–58.
(72) Lammel, G.; Renaud, P. *Sens. Actuators, A* **2000**, *85*, 356–360.
(73) Song, J. H.; Sailor, M. J. *J. Am. Chem. Soc.* **1997**, *119*, 7381–7385.
(74) Starodub, V. M.; Fedorenko, L. L.; Sisetskiy, A. P.; Starodub, N. F. *Sens. Actuators, B* **1999**, *58*, 409–414.
(75) Jane, A.; Dronov, R.; Hodges, A.; Voelcker, N. H. *Trends Biotechnol.* **2009**, *27*, 230–239.
(76) Buriak, J. M. *Chem. Commun.* **1999**, 1051–1060.
(77) Stewart, M. P.; Buriak, J. M. *J. Am. Chem. Soc.* **2001**, *123*, 7821–7830.
(78) Lees, I. N.; Lin, H.; Canaria, C. A.; Gurtner, C.; Sailor, M. J.; Miskelly, G. M. *Langmuir* **2003**, *19*, 9812–9817.
(79) Guo, D. J.; Xiao, S. J.; Xia, B.; Wei, S.; Pei, J.; Pan, Y.; You, X. Z.; Gu, Z. Z.; Lu, Z. *J. Phys. Chem. B* **2005**, *109*, 20620–8.
(80) Giovannozzi, A. M.; Rocchia, M. *Sens. Actuators, B* **2008**, *130*, 795–801.
(81) Yang, M.; Teeuwen, R. L. M.; Giesbers, M.; Baggerman, J.; Arafat, A.; Wolf, F. A. d.; Hest, J. C. M. v.; Zuilhof, H. *Langmuir* **2008**, *24*, 7931–7938.
(82) Bocking, T.; Kilian, K. A.; Gaus, K.; Gooding, J. J. *Adv. Funct. Mater.* **2008**, *18*, 3827–3833.
(83) Innocenti, A.; Casini, A.; Alcaro, M. C.; Papini, A. M.; Scozzafava, A.; Supuran, C. T. *J. Med. Chem.* **2004**, *47*, 5224–5229.
(84) Koepsel, J. T.; Murphy, W. L. *Langmuir* **2009**, *25*, 12825–12834.
(85) Andruzzi, L.; Senaratne, W.; Hexemer, A.; Sheets, E. D.; Ilic, B.; Kramer, E. J.; Baird, B.; Ober, C. K. *Langmuir* **2005**, *21*, 2495–2504.